



LJMU Research Online

Wang, YC, Lai, HW and Ren, XJ

Enhanced Auxetic and Viscoelastic Properties of Filled Reentrant Honeycomb

<http://researchonline.ljmu.ac.uk/id/eprint/12059/>

Article

Citation (please note it is advisable to refer to the publisher's version if you intend to cite from this work)

Wang, YC, Lai, HW and Ren, XJ (2019) Enhanced Auxetic and Viscoelastic Properties of Filled Reentrant Honeycomb. Physica Status Solidi (B) Basic Research. ISSN 0370-1972

LJMU has developed **LJMU Research Online** for users to access the research output of the University more effectively. Copyright © and Moral Rights for the papers on this site are retained by the individual authors and/or other copyright owners. Users may download and/or print one copy of any article(s) in LJMU Research Online to facilitate their private study or for non-commercial research. You may not engage in further distribution of the material or use it for any profit-making activities or any commercial gain.

The version presented here may differ from the published version or from the version of the record. Please see the repository URL above for details on accessing the published version and note that access may require a subscription.

For more information please contact researchonline@ljmu.ac.uk

<http://researchonline.ljmu.ac.uk/>

Enhanced Auxetic and Viscoelastic Properties of Filled Reentrant Honeycomb

Yun-Che Wang,* Hsiang-Wei Lai, and Xuejun James Ren

Dr. Y.-C. Wang, H.-W. Lai,

Department of Civil Engineering, National Cheng Kung University, 1 University Road, Tainan 70101, Taiwan, R.O.C.

E-mail: yunche@mail.ncku.edu.tw.

Dr. X. J. Ren

Department of Mechanical and Maritime Engineering, Faculty of Engineering and Technology, Liverpool John Moores University, Liverpool L3 3AF, UK

Abstract:

Honeycombs or foams with reentrant microstructures exhibit effective negative Poisson's ratio. Although they are light weight due to inherently empty space, their overall stiffness and damping are somewhat limited. With judiciously chosen filler material to fill the voids in star-shaped honeycomb, it is numerically demonstrated its auxeticity may be enhanced. By combining the filler and skeleton, the hierarchical composite materials are constructed. The magnitude of the enhancement depends on inner and outer filler's modulus mismatch, as well as the types of filling. Filler's auxeticity also largely enhances overall auxeticity of the outer- and all-filled honeycomb. In addition, for outer-filled honeycomb, its effective viscoelastic modulus and damping are significantly increased, while maintaining relatively light weight, due to local stress concentration.

Keywords: auxetic materials, finite element method, negative Poisson's ratio, star-shaped honeycombs, viscoelasticity

1. Introduction

Foam-based negative Poisson's ratio (NPR) materials, including reentrant honeycombs, contain macroscopic voids.[1] Auxetic materials may also be obtained through network design at molecular levels.[2] Mechanical responses of the auxetic materials have been reported in accordance with the prediction of the elasticity theory.[3,4] For materials with anisotropy, partial auxeticity, i.e., NPR along certain loading directions, may be more commonly observed.[5] Atomic analysis has shown that FCC hard sphere models containing certain type of planar defects may lead to directional NPR phenomena.[6] Recently, 2D NPR systems containing star-shaped microstructures with square symmetry have been systematically studied for their effective elastic properties.[7] The effective Young's modulus and Poisson's ratio of planar structures containing elliptic inclusions, also with the square symmetry, have been investigated in detail by Pozniak et al.[8] In addition, many studies have been conducted to obtain basic understanding of the 2D auxetic materials and systems.[9-11].

In addition to the reentrant cell shape as a mechanism to obtain NPR, other mechanisms have been investigated, such as connected stars,[12] connected rectangles,[13] and rotating units related structures.[14]. All of the mechanisms require empty space, i.e., voids, inside the material. It has been shown that phase-transformation-induced negative bulk modulus may lead to NPR in continuum without voids.[15] Furthermore, NPR may be observed in isotropic alloys near a morphotropic boundary due to phase transition.[16] In this work, our filled honeycombs also demonstrate the attainability of NPR materials with no need of empty space.

NPR materials are distinct from negative stiffness (NS) materials, though some materials or systems may simultaneously exhibit NPR and NS.^[17–19] The inter-relations between negative compressibility and NPR have been demonstrated that they are attainable.^[20] Using the phase field modeling, NS effects have been examined without directly assigning negative modulus values in calculations.^[21,22] In addition, NS effects on the overall viscoelastic and coupled field properties have been investigated with the finite element analysis.^[23] Furthermore, energy dissipation of a viscoelastic composite beam-column connector has been numerically analyzed to exhibit its high stiffness and high damping^[24].

In this work, we adopt the finite element method (FEM)^[25] to numerically study the effective Poisson's ratio of filled, re-entrant honeycomb for their in-plane elastic properties. In addition, effects on the linear viscoelastic properties due to the filling and local stress concentration are discussed. The system studied in this work is of square symmetry; not isotropic. Effective properties of the system under the loading along a symmetry axis are investigated.

2. Elasticity Modeling

For an isotropic and homogeneous elastic solid, its displacement field \mathbf{u} is governed by the Navier equation, as follows.^[26]

$$\mu \nabla^2 \mathbf{u} + (\lambda + \mu) \nabla (\nabla \cdot \mathbf{u}) + \rho \mathbf{b} = \rho \mathbf{a} \quad (1)$$

where ρ , \mathbf{a} , \mathbf{b} are density, acceleration vector, and body force vector, respectively. The gradient and Laplacian operator are denoted by ∇ and ∇^2 , respectively. The shear modulus is denoted by μ and Lamé constant λ . They are related to Young's modulus E through $\lambda = \mu(E - 2\mu)/(3\mu - E)$. For isotropic and homogeneous media, Poisson's ratio $\nu = E/2G - 1$, where the symbols G and μ are used interchangeably for shear modulus. We adopt the FEM to numerically solve Equation (1) with suitable loading and boundary conditions to calculate the effective elastic Young's modulus and Poisson's ratio of the honeycomb under the plane strain conditions, provided with $\mathbf{a} = \mathbf{b} = \mathbf{0}$. The solid phase of the honeycomb is assumed to have Young's modulus of 100MPa and Poisson's ratio of 0.3. In our finite element calculations for the elastic properties, loading on the boundaries is under displacement control. Although we assume isotropy in the solid phases, the overall responses of the structures are not isotropic. They are of square symmetry due to the arrangements of the ribs.

The effective properties of the honeycomb are calculated in terms of volume-averaged stress ($\bar{\sigma}_{ij}$) and strain ($\bar{\epsilon}_{ij}$). When the sample is under straining along the horizontal direction, i.e., x-direction, its effective Young's modulus and Poisson's ratio of the honeycomb are, respectively, calculated by

$$E_{\text{eff}} = \frac{\bar{\sigma}_{xx}}{\bar{\epsilon}_{xx}} \quad (2)$$

$$\nu_{\text{eff}} = -\frac{\bar{\epsilon}_{yy}}{\bar{\epsilon}_{xx}} \quad (3)$$

The volume-averaged stress and strain are defined as follows:[27]

$$\bar{\sigma}_{ij} = \frac{1}{V} \int_{\Omega} \sigma_{ij} dV = \frac{1}{V} \int_{\partial\Omega} t_j x_i dA \quad (4)$$

$$\bar{\epsilon}_{ij} = \frac{1}{V} \int_{\Omega} \epsilon_{ij} dV = \frac{1}{2V} \int_{\partial\Omega} (u_i n_j + u_j n_i) dA \quad (5)$$

Here Ω indicates the domain of material, $\partial\Omega$ the boundary of the domain, V the volume of the domain, and A the surface surrounding the domain. The traction, displacement, and unit vector of associated boundaries are, respectively, denoted by t_i , u_i , and n_i . Supported by Equation (4)

and (5), we calculated the average stress and strain on the boundary of the domain to evaluate the effective elastic properties of the honeycomb.

3. Viscoelasticity Modeling

For the viscoelastic calculations, the relaxed bulk modulus (K) and shear modulus (G) of the solid phase are assumed to be 83.33, and 38.46 MPa, respectively. This choice of moduli correspond to the Young's modulus and Poisson's ratio used in the elasticity calculations, i.e., 100 MPa and 0.3, respectively. For the linear viscoelastic case, the shear behavior of the solid phase is governed by the standard linear solid (SLS) model, as shown in Equation (6), whereas the bulk behavior is assumed to be purely elastic, Equation (7).

$$s_{ij} + T_1 \frac{ds_{ij}}{dt} = G \left(e_{ij} + T_2 \frac{de_{ij}}{dt} \right), \quad i \neq j \quad (6)$$

$$\sigma_{kk} = 3K e_{kk} \quad (7)$$

Here, the deviatoric stress is denoted by $s_{ij} = \sigma_{ij} - \sigma_{kk}/3$, and deviatoric strain $e_{ij} = \epsilon_{ij} - \epsilon_{kk}/3$. Time derivative is indicated by d/dt . The time constants are $T_1=0.1s$, and $T_2=T_1(G+G_1)/G=1.5T_1$, where G_1 is the shear modulus of the viscoelastic branch in the SLS model and is assumed to be $G/2=19.23$ MPa. The choice of these material parameters is representative to include linear viscoelastic effects in the FEM with suitable frequency dependence.^[28] Figure 1a,b shows the frequency-dependent viscoelastic modulus and loss tangent of the solid phase of the plates. We remark that the effective properties of the microstructured plates may be different from those of the solid-phase material due to the composite effects between the solid phase and empty space through the cell size and cell shape effects. All of our finite element calculations for effective viscoelastic properties are under load control.

$$W_s = \frac{1}{2} \sigma_{ij} \epsilon_{ij} \quad (8)$$

$$W_d = \int_0^T \sigma_{ij} \frac{d\epsilon_{ij}}{dt} dt \quad (9)$$

As for calculating the effective linear viscoelastic properties of the honeycomb, we apply low frequency (1 Hz) sinusoidal loading on the boundaries throughout this work, and calculate the stress-strain Lissajous curve of the honeycomb. The width and slope of the Lissajous curve may yield the information about the effective loss tangent and the absolute value of complex modulus, respectively.^[29]

4. Numerical Considerations

In the 2D, plane-strain, finite element calculations, we adopt the triangular elements to form the mesh. Typical mesh is shown in Figure 2. Figure 2b,d,f are the zoom-ins of Figure 2a,c,e. The quadratic Lagrange shape function is used to interpolate field quantities within an element. The numbers of triangular elements for the three honeycomb models, i.e., inner-filled, outer-filled, and all-filled honeycomb, studied in this work are shown in Table 1. The numbers of degrees of freedom (DOF) for the elastoelastic and viscoelastic analysis are listed in Table 2. To avoid singularities at the sharp geometric corners between ribs, all corners are smoothed so that every point in the domain is at least twice differentiable.^[24,30]

5. Results and Discussion

5.1. Effects of Filler's Modulus

When the Young's modulus of the inner filler (E_i) is chosen to be the same as that of the outer filler (E_o), the variations of effective Poisson's ratio of the honeycomb on the filler-to-skeleton Young's modulus ratio ER is shown in Figure 3. The definition of the Young's modulus ratio

is $E_R = E_i/E_s$, or $E_R = E_o/E_s$, depending on if the bare honeycomb is inner-filled or outer-filled. The Young's modulus of the honeycomb skeleton is denoted by E_s , and is set to be 100 MPa. For the all-filled honeycomb, $E_R = E_i/E_s = E_o/E_s$. Effects of the all-filled case with $E_i \neq E_o$ are discussed along with Figure 4. The filler's Poisson's ratio is assumed to be 0.3. When the honeycomb is not filled at all, its effective Young's modulus $E_{xx} = 6.26$ kPa and Poisson's ratio $\nu_{eff} = -\epsilon_{yy}/\epsilon_{xx} = -0.492$, has been previously obtained.^[7] The enhancement observed in the partially filled model can be contributed to from the hierarchical effects.^[31]

As shown in the figure, when E_R is about 10^{-4} , the outer-filled honeycomb shows the lowest effective Poisson's ratio (-0.65). When E_o is equal to E_s , i.e., $E_R = 1$, the outer-filled honeycomb exhibits slightly positive Poisson's ratio ($\nu_{eff} = 0.0473$). For the all-filled model, a minimum Poisson's ratio occurs at $E_R = 10^{-5}$, with $\nu_{eff} = -0.485$. When the filler is placed in the stars in bare honeycomb (inner-filled case), the effective Poisson's ratio shows a non-decreasing feature as E_R increases. When $E_R = 10^{-3}$, the inner-filled honeycomb shows a maximum effective Poisson's ratio $\nu_{eff} = 0.392$. When $E_R = 1$, the effective Poisson's ratio of the all-filled honeycomb reaches a maximum of $\nu_{eff} = 0.429$, and the model contains no empty space. Furthermore, as the filler's Young's modulus and Poisson's ratio are identical to those of the skeleton, it is impossible to distinguish the two phases. Therefore, the $E_R = 1$ model behaves as an isotropic and homogeneous material with Young's modulus 100 MPa and Poisson's ratio 0.3. It is remarked that in general the structure is of square symmetry when E_R is not equal to 1. The maximum Poisson's ratio value 0.429 is different from 0.3 as the honeycomb is analyzed under the plane strain assumption. It is remarked that zero effective Poisson's ratio may be obtained from all of the three filled honeycomb models by suitably choosing E_i , E_o , or both. To examine the effects of the Young's modulus of the honeycomb skeleton, Figure 5a shows the effective Poisson's ratio of the all-filled honeycomb with two different skeleton Young's modulus $E_s = 100$ MPa or $E_s = 100$ GPa. In both cases, the Poisson's ratio of the skeleton is set to be 0.3. After normalization on the filler modulus, the two cases show identical effective Poisson's ratio versus E_n curve, indicating the systems can be scaled, as expected. The definition of E_n is as follows. For $E_s = 100$ MPa, the normalization factor is 1000 and $E_n = E_i/1000 = E_o/1000$. For $E_s = 100$ GPa, 10^6 is chosen as the normalization factor and $E_n = E_i/10^6 = E_o/10^6$.

For the all-filled model, previous discussions focus on the $E_i = E_o$ scenario, Figure 4 shows the effective Poisson's ratio of the all-filled honeycomb when $E_i \neq E_o$. We define the Young's modulus ratio $E_p = E_o/E_i$, where E_i is set to be 10 kPa. The Young's modulus of the skeleton is $E_s = 100$ MPa. The Poisson's ratio of the inner and outer filler, as well as the skeleton, is assumed to be the same and equals to 0.3. As can be seen, the lowest effective Poisson's ratio ($\nu_{eff} = 0.548$) occurs at $E_p = 10$. When $E_o \gg E_i$ or $E_o \ll E_i$, the effective Poisson's ratio becomes positive. With this finding, one may design material with any Poisson's ratio by suitably choosing the inner and outer filler.

5.2. Effects of Filler's Poisson's Ratio

When the Young's modulus of the filler material fixed ($E_i = E_o = 1$ kPa), Figure 6 shows the effective Poisson's ratio (ν_{eff}) of the filled honeycombs versus the Poisson's ratio (ν) of the filler material. As can be seen, for the outer-filled and all-filled honeycomb, more negative ν would lead to more negative ν_{eff} . However, for the inner-filled case, the lowest ν_{eff} ($= -0.3972$) occurs at $\nu = -0.12$. Based on the trend of the data, when ν approaches 0.5, ν_{eff} becomes positive for all cases studied here.

5.3. Effective Viscoelastic Properties

In the aforementioned studies, all materials, including the skeleton, inner, and other filler, are all elastic. In this section, we assume the skeleton is still elastic, but the filler materials are linearly viscoelastic. It is remarked that although the idea of using viscoelastic infills in foam has existed,^[32] our work here explicitly and quantitatively demonstrate the viscoelastic effects in the all filled or partially filled auxetic structures. Figure 7 shows the stress–strain Lissajous of the systems under a few cycles of sinusoidal loading at 1 Hz. Transient responses exist in all three cases, and can be clearly observed in Figure 7b. The effective stress and strain are measured at the loading edge, i.e., the right edge of the square domain in Figure 2a,c,e. The maximum applied stresses (σ_{xx})_{max} are chosen differently to ensure small strain in the samples on the same order of magnitude about 10^{-6} . The viscoelastic modulus and loss tangent are calculated from the Lissajous curves, after the transient responses are removed. The all-filler honeycomb exhibits largest viscoelastic modulus and damping ($|E^*|= 120.965$ MPa and $\tan \delta=0.1299$), as shown in Figure 7a. The inner-filled case shows the smallest modulus and damping ($|E^*|=3.125$ MPa and $\tan \delta = 0.0106$). Comparing the bare honeycomb, which is purely elastic and has effective Young's modulus 6.26 kPa, the filled honeycombs show large enhancements in effective modulus and damping. It is remarked that for light-weight applications, the outer-filled honeycomb has more enhanced viscoelastic modulus and damping than the inner-filled one. From Equation (8) and (9), the calculated storage and dissipation energy density are shown in Figure 8a–c for the all-filled, outer-filled, and inner-filled honeycomb under 1 Hz sinusoidal stressing along the x-direction. Both the left and right vertical axes are in logarithmic scale. The accumulation of the dissipation energy density (blue dashed curves) increases with time in the step-like manner. Storage energy reaches zero at half of loading period because of zero strain. As shown in Figure 8b, the outerfilled case shows largest storage and dissipation energy density due to large local stress concentration with the magnitude of 400 Pa in terms of von Mises average stress, as shown in Figure 9b. The external applied stresses σ_{xx} for Figure 9a–c are, respectively, 99.898, 100.22, and 1.894 Pa, as shown in Figure 7. These applied stresses are chosen so that the strain on the loading edge is on the order of 10^{-6} . The all-filled honeycomb does not show strong local stress concentration. Although stress concentration is identifiable in the inner-filled honeycomb, its magnitude is small due to its overall Young's modulus is small, so that to maintain similar deformation, the applied stress is much smaller, as compared with the other two filled honeycombs. Therefore, the energy dissipation capability of the inner-filled honeycomb is not significantly improved.

6. Conclusions

The auxeticity of honeycomb with reentrant microstructures may be enhanced by judiciously filling the voids. The outer-filled honeycomb with $ER = 10^{-4}$ shows a 32% increase in the negativity of the Poisson's ratio, i.e., from -0.492 to -0.65. For all-filled honeycomb with $E_p = 10$, a smallest effective Poisson's ratio about -0.55 can be achieved. Effects of structural hierarchy play a role in the enhancement of auxeticity. When the filler is made of auxetic material, the outer- and all-filled honeycombs show strongly enhanced effective NPR as the filler toward more auxetic. The inner-filled honeycomb shows the lowest effective Poisson's ratio at filler's Poisson's ratio equal to -0.12. Overall viscoelastic modulus and damping are largely enhanced in the all-filled and outer-filled honeycomb. Considering low weight, the outer-filled honeycomb has more enhanced viscoelastic modulus and damping than the inner-filled one. Significant local stress concentration in the outer-filled honeycomb leads to larger energy dissipation properties.

Acknowledgements

X.J.R. and Y.-C.W. acknowledge the support from the Royal Society International exchange Project IE1609966. Y.-C.W. acknowledges support from the Ministry of Science and Technology, Taiwan, with grant number MOST 107-2221-E-006-028. This research was, in part, supported by the Ministry of Education, Taiwan, R.O.C, and the Aim for the Top University Project to the National Cheng Kung University (NCKU). The authors are grateful to the National Center for High-Performance Computing, Taiwan, for computer time and facilities.

Conflict of Interest

The authors declare no conflict of interest

- [1] R. S. Lakes, *Science* 1987, 235, 1038.
- [2] K. E. Evans, M. A. Nkansah, I. J. Hutchinson, S. C. Rogers, *Nature* 1991, 353, 124.
- [3] R. Lakes, *Adv. Mater.* 1993, 5, 293.
- [4] T.-C. Lim, *Auxetic Materials and Structures*, Springer, Berlin / New York 2015.
- [5] K. W. Wojciechowski, *Comput. Methods Sci. Technol.* 2005, 11, 73.
- [6] J. W. Narojczyk, K. W. Wojciechowski, *Materials* 2019, 12, 700.
- [7] Y. C. Wang, M. W. Shen, S. M. Liao, *Phys. Status Solidi B* 2017, 254, 1700024.
- [8] A. A. Pozniak, K. W. Wojciechowski, J. N. Grima, L. Mizzi, *Composites, Part B* 2016, 94, 379.
- [9] K. W. Wojciechowski, *J. Phys. Soc. Jpn.* 2003, 72, 1819.
- [10] K. W. Wojciechowski, *Mol. Phys.* 1987, 61, 1247.
- [11] K. W. Wojciechowski, *Phys. Lett. A* 1989, 137, 60.
- [12] J. N. Grima, R. Gatt, A. Alderson, K. E. Evans, *Mol. Simul.* 2005, 31, 925.
- [13] J. N. Grima, E. Manicaro, D. Attard, *Proc. R. Soc. A* 2011, 467, 439.
- [14] L. Mizzi, K. M. Azzopardi, D. Attard, J. N. Grima, R. Gatt, *Phys. Status Solidi RRL* 2015, 9, 425.
- [15] Y. C. Wang, R. S. Lakes, *J. Compos. Mater.* 2005, 39, 1645.
- [16] D. Li, T. Jaglinski, D. S. Stone, R. S. Lakes, *Appl. Phys. Lett.* 2012, 101, 251903.
- [17] T. M. Jaglinski, R. S. Lakes, *Adaptive Structures: Engineering Applications* (Eds: D. Wagg, I. Bond, P. Weaver, M. Friswell), John Wiley & Sons, Chichester, England 2007, pp. 231–246.
- [18] S. Xinchun, R. S. Lakes, *Phys. Status Solidi B* 2007, 244, 1008.
- [19] T. A. M. Hewage, K. L. Alderson, A. Alderson, F. Scarpa, *Adv. Mater.* 2016, 28, 10323.
- [20] R. Lakes, K. W. Wojciechowski, *Phys. Status Solidi B* 2008, 245, 545.
- [21] Y. C. Wang, M. W. Shen, *Phys. Status Solidi B* 2016, 253, 1428.
- [22] Y. C. Wang, H. W. Lai, M. W. Shen, *Phys. Status Solidi B* 2019, 256, 1800489.
- [23] Y. C. Wang, C. C. Ko, K. W. Chang, *Phys. Status Solidi B* 2015, 252, 1640.
- [24] Y. C. Wang, C. C. Ko, *Steel Compos. Struct.* 2015, 18, 1161.
- [25] R. D. Cook, D. S. Malkus, M. E. Plesha, R. J. Witt, *Concepts and Applications of Finite Element Analysis*, 4th ed., John Wiley & Sons,

Chichester, England 2001.

[26] R. W. Soutas-Little, *Elasticity*, Dover, New York 1973.

[27] R. Lakes, W. Drugan, *J. Mech. Phys. Solids* 2002, 50, 979.

[28] Y. C. Wang, C.-C. Ko, *Phys. Status Solidi B* 2013, 250, 2070.

[29] R. Lakes, *Viscoelastic Materials*, Cambridge University Press, New York, NY 2009.

[30] COMSOL website, <http://www.comsol.com> (accessed: February 2019).

[31] R. Lakes, *Nature* 1993, 361, 511.

[32] F. K. A. El-Sayed, R. Jones, I. W. Burgess, *Composites* 1979, 10, 209.

Table 1. Number of triangular elements used in the FEM mesh of the three honeycomb models. The mesh is shown in Figure 2.

Type	Inner-filled	Outer-filled	All-filled
Number of elements	75 928	66 986	10 9388

Table 2. FEM DOF of the three honeycomb models.

Type	Inner-filled	Outer-filled	All-filled
Displacement field	313 066	273 664	439 006
Viscoelastic field quantities	376 680	501 810	877 920

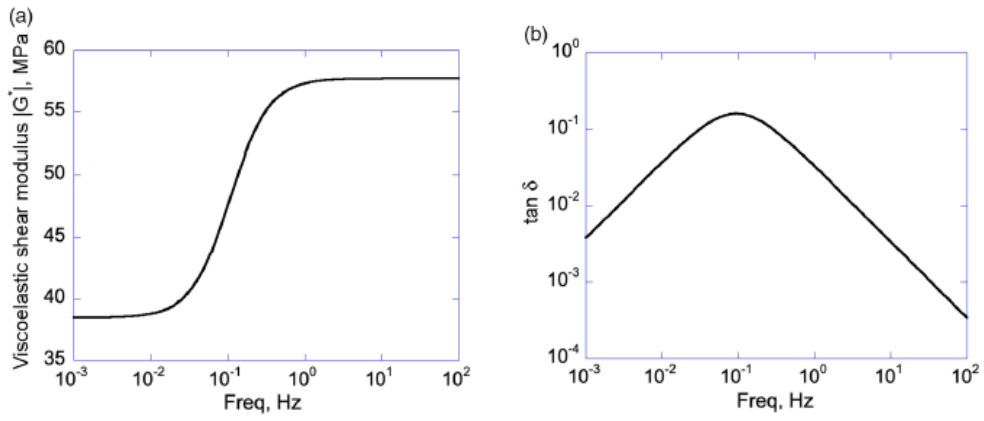


Figure 1. Frequency response of the a) absolute value of the viscoelastic shear modulus and b) $\tan \delta$ of the SLS model used for the solid phase of the microstructured discs.

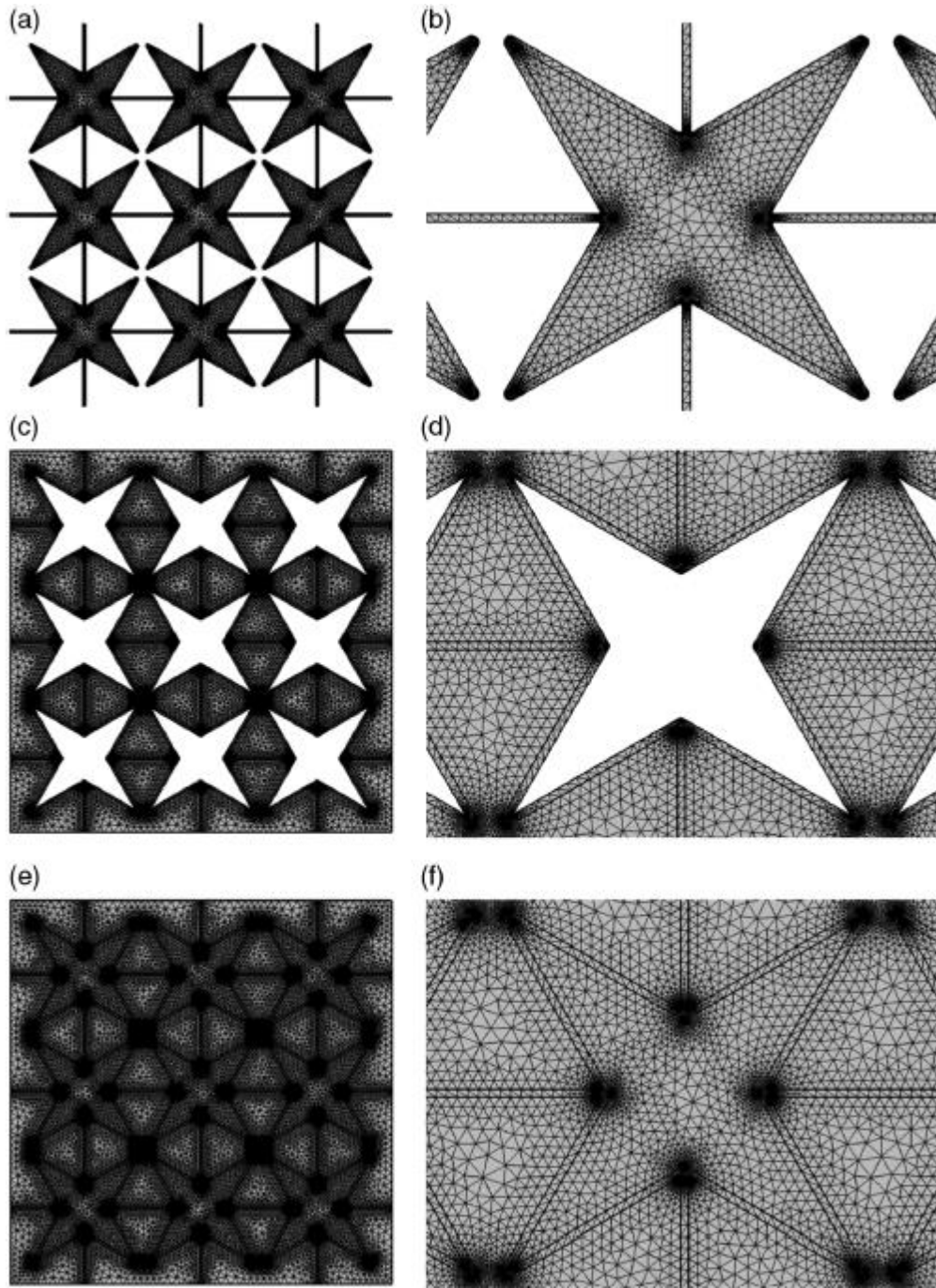


Figure 2. Finite element mesh used in this study a,b) for the inner-filled, c,d) outer-filled, and e,f) all-filled honeycomb model. The edge length of the square domain is 15 cm. The roller boundary conditions are assigned to the left and bottom edges of the samples.

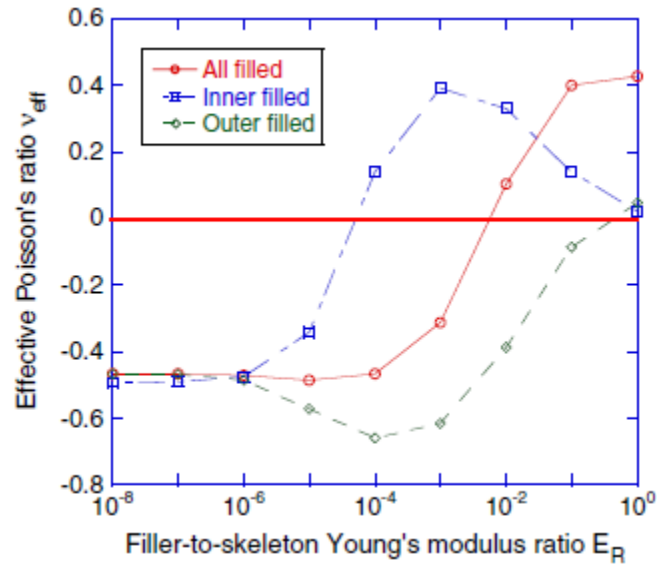


Figure 3. Effective Poisson's ratio versus Young's modulus ratio E_R . The definitions of E_R are as follows. $E_R = E_i/E_s$ for the inner filled honeycomb, $E_R = 1/4 E_o/E_s$ for the outer-filled honeycomb, $E_R = E_i/E_s = E_o/E_s$ for all empty space filled honeycomb when $E_i = E_o$. The Young's modulus of the honeycomb ribs, E_s , is set to be 100 MPa.

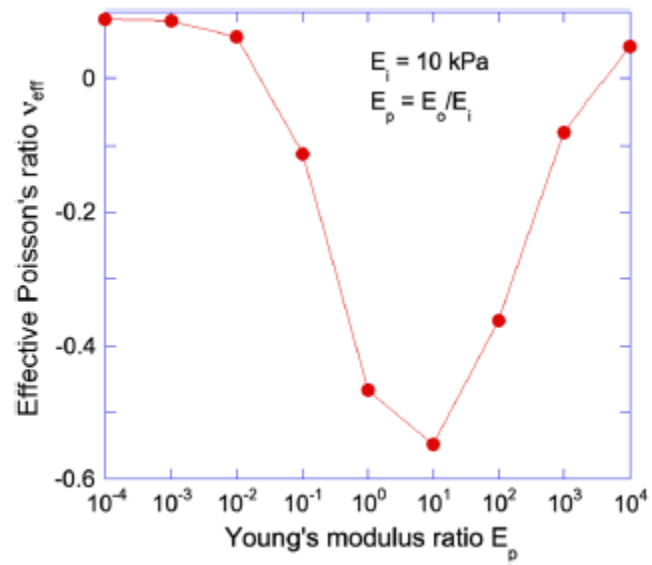


Figure 4. Effective Poisson's ratio versus modulus ratio $E_p = E_o/E_i$, whereas E_i is fixed to 10 kPa and the Young's modulus of the honeycomb ribs is $E_s = 100 \text{ MPa}$.

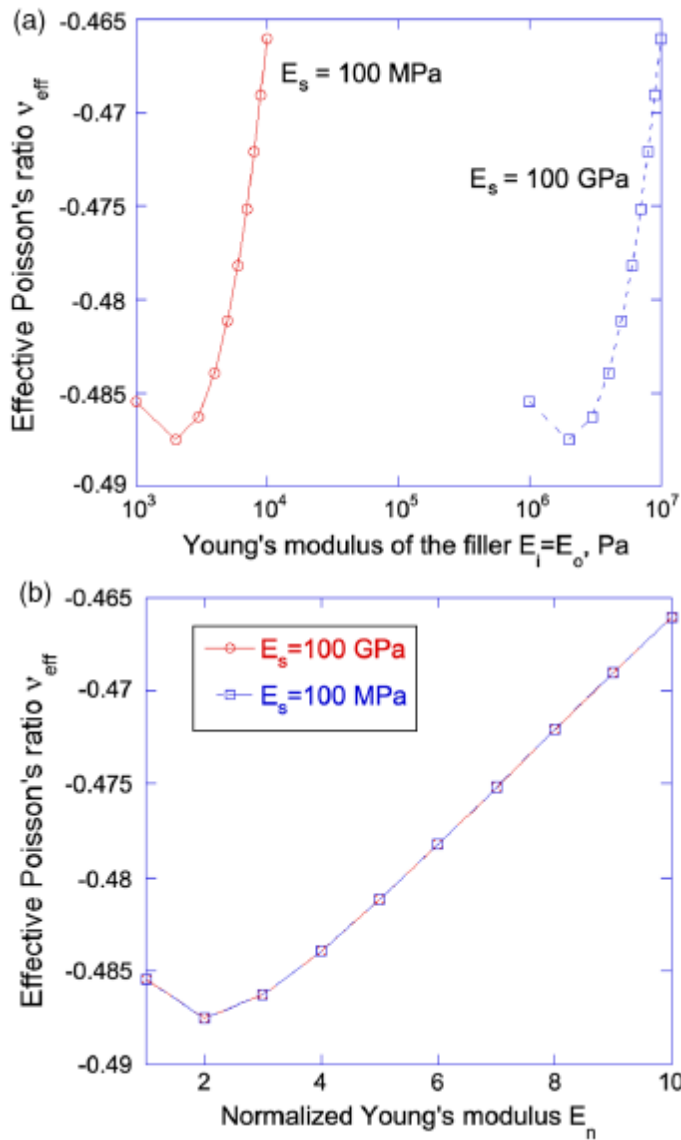


Figure 5. a) Effective Poisson's ratio versus filler modulus for the honeycomb with all empty space filled by same material, and b) effective Poisson's ratio versus normalized filler modulus under two different Young's modulus for the skeleton. The definition of normalized Young's modulus is stated in the text.

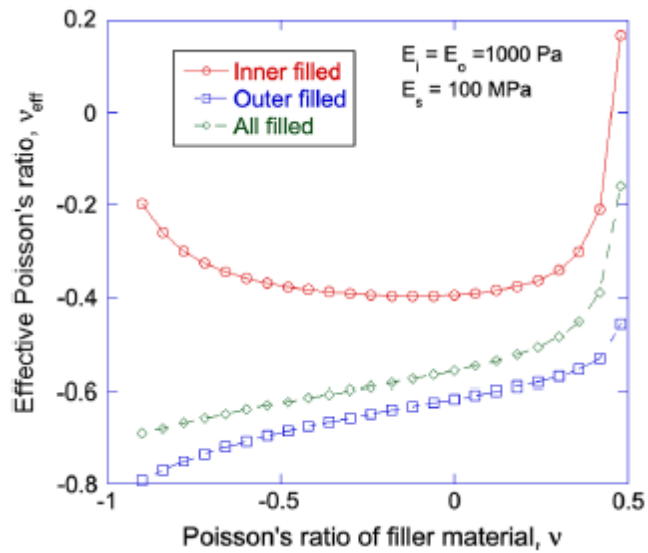


Figure 6. Effective Poisson's ratio of the honeycomb with various filler Poisson's ratio. The lowest effective Poisson's ratio of the inner-filled honeycomb is $v_{\text{eff}} \approx -0.3972$ at the filler's Poisson's ratio $v = -0.12$.

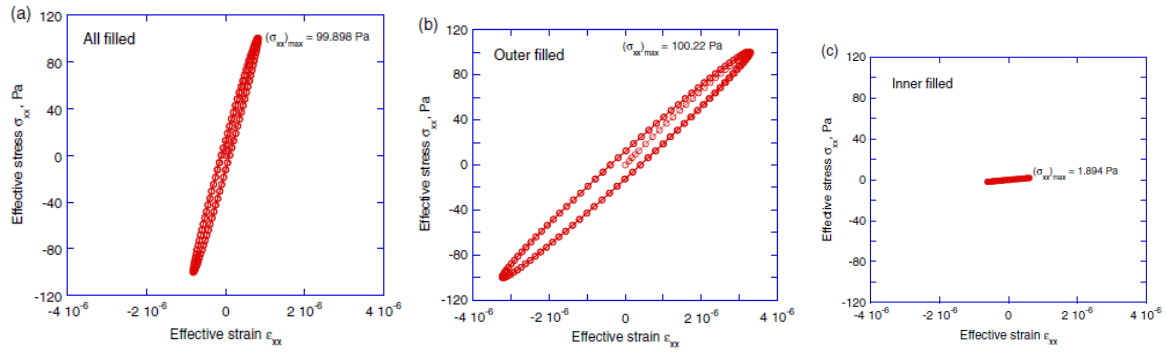


Figure 7. Stress–strain Lissajous curves of the a) all-filled, b) outer-filled, and c) inner-filled honeycomb at 1 Hz. Effective viscoelastic properties are as follows: a) $\tan \delta = 0.1299$, $|E^*| = 120.965 \text{ MPa}$, b) $\tan \delta = 0.1219$, $|E^*| = 30.699 \text{ MPa}$, and c) $\tan \delta = 0.0106$, $|E^*| = 3.125 \text{ MPa}$. The skeleton of the reentrant honeycomb is elastic, and the effective Young’s modulus of the bare honeycomb is 6.26 kPa.

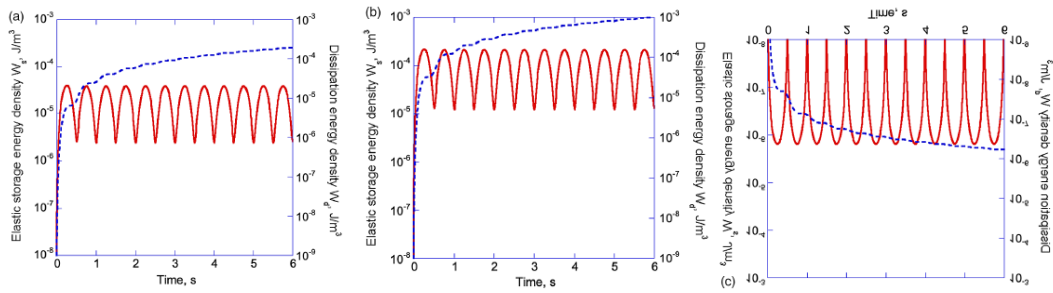


Figure 8. Storage and dissipation energy density of the a) all-filled, b) outer-filled, and c) inner-filled honeycomb driven at 1 Hz. Red solid curves are for the storage energy density, and blue dashed curves for the dissipation energy density.

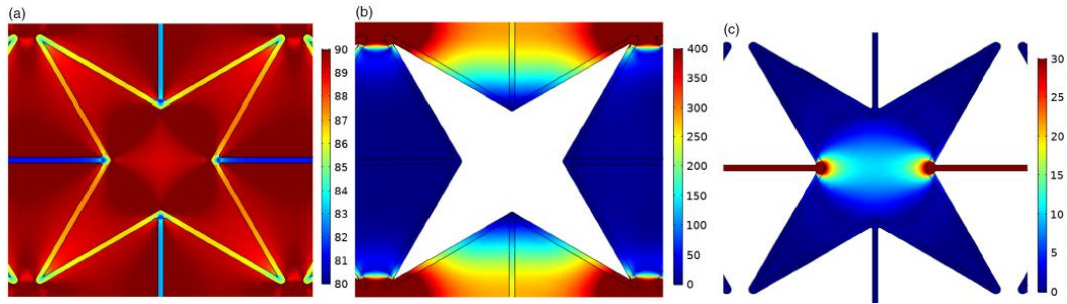


Figure 9. von Mises stress distributions in the a) all-filled, b) outer-filled, and c) inner-filled honeycomb at $(\sigma_{xx})_{\max}$, indicated in Figure 7. Color bars are in units of Pa.